Bilayer Properties of Lipid A from Various Gram-Negative Bacteria

Seonghoon Kim,[1] Dhilon S. Patel,[1] Soohyung Park,[1] Joanna Slusky,[2] Jeffery B. Klauda,[3] Göran Widmalm,[4] and Wonpil Im[1,*]

[1]Department of Biological Sciences and Bioengineering Program, Lehigh University, Bethlehem, Pennsylvania; [2]Department of Molecular Biosciences and Center for Computational Biology, The University of Kansas, Lawrence, Kansas; [3]Department of Chemical and Biomolecular Engineering and the Biophysics Program, University of Maryland, College Park, Maryland; and [4]Department of Organic Chemistry, Arrhenius Laboratory, Stockholm University, Stockholm, Sweden

ABSTRACT   Lipid A is the lipid anchor of a lipopolysaccharide in the outer leaflet of the outer membrane of Gram-negative bacteria. In general, lipid A consists of two phosphorylated *N*-acetyl glucosamine and several acyl chains that are directly linked to the two sugars. Depending on the bacterial species and environments, the acyl chain number and length vary, and lipid A can be chemically modified with phosphoethanolamine, aminoarabinose, or glycine residues, which are key to bacterial pathogenesis. In this work, homogeneous lipid bilayers of 21 distinct lipid A types from 12 bacterial species are modeled and simulated to investigate the differences and similarities of their membrane properties. In addition, different neutralizing ion types (Ca^{2+}, K^+, and Na^+) are considered to examine the ion's influence on the membrane properties. The trajectory analysis shows that (1) the area per lipid is mostly correlated to the acyl chain number, and the area per lipid increases as a function of the acyl chain number; (2) the hydrophobic thickness is mainly determined by the average acyl chain length with slight dependence on the acyl chain number, and the hydrophobic thickness generally increases with the average acyl chain length; (3) a good correlation is observed among the area per lipid, hydrophobic thickness, and acyl chain order; and (4) although the influence of neutralizing ion types on the area per lipid and hydrophobic thickness is minimal, Ca^{2+} stays longer on the membrane surface than K^+ or Na^+, consequently leading to lower lateral diffusion and a higher compressibility modulus, which agrees well with available experiments.

INTRODUCTION

Lipopolysaccharides (LPS) are an integral component of the outer leaflet of the outer membrane of Gram-negative bacteria where they function/act as a shield and barrier to environmental threats to the bacterium. The study of LPS and the overall outer membrane shape and structure is important because LPS structure can inform outer membrane protein biogenesis and antibiotic design. The shape and stability of the outer membrane is believed to play a large part in the insertion and folding of outer membrane proteins (1,2). Moreover, it is the LPS that make the outer membrane more impermeable to antibiotics (3), so understanding and then manipulating LPS membrane stability would be a rational way to develop new Gram-negative antibiotics.

In contrast to the difficulties in studying the membrane structure of LPS, the chemical structure of LPS has been studied in detail, largely owing to mass spectrometry techniques. The LPS is built of three regions: the O-antigen polysaccharide, the core, and lipid A. The O-antigen polysaccharide is highly variable and is the basis for serogroup determination of bacteria. This outermost region extends out from the membrane and is composed of repeating units of oligosaccharides, typically consisting of five sugar residues and repeated up to 25 times (although longer O-chains are present in some cases). The second region is the intermediate structural region referred to as the core. This region consists of an oligosaccharide of up to a dozen sugar residues and is relatively conserved within a species. The final, anchoring region is known as lipid A and consists of a β-(1→6)-linked disaccharide that is acylated with up to eight fatty acids of different lengths and complexities as well as charged substituents such as phosphate groups, phosphoethanolamine residues, or positively charged sugar residues (4).

It is the lipid A that is responsible for the toxic effects of Toxic Shock Syndrome and sepsis. There are many variations within lipid A of different bacteria species. The disaccharide of lipid A most often contains D-glucosamine residues, but in some species 3-amino-3-deoxy-D-glucosamine is present

CrossMark

instead. The acylation at positions 2 and 2′ of the disaccharide (reducing and terminal sugar residue, respectively) leads to amide-linked lipids, which is also the case for the 3- and 3′-positions when the 3-amino-3-deoxy-D-glucosamine is acylated. The hydroxyl groups at positions 3 and 3′ as well as the 3-hydroxyl group of the fatty acyl chains are also acylated, resulting in ester-linked substituents. The extent of acylation with 4–8 acyl groups attached to the β-(1→6)-linked disaccharide varies between species and more than a single form is often present in the lipid A from a certain bacterial species.

In the canonical form of lipid A, there is substitution by phosphoryl groups at the 1- and 4′-positions of the disaccharide, a modification that gives the molecule an overall negative charge. However, this makes it prone to binding of positively charged cationic antimicrobial peptides and, to evade attack by the immune system, some bacteria have developed structural modifications with less negative charge (4). To facilitate this, phosphoryl groups are either removed or decorated as phosphoethanolamine or pyrophosphoethanolamine entities or with a phosphodiester-linked sugar, e.g., 4-amino-4-deoxy-β-L-arabinopyranose. Based on the same theme, ester-linked amino acids (glycine) substitute position 3 of fatty acid chains in lipid A in some cases, which results in a free amino group, thereby decreasing the overall charge of the lipid A.

In this study, homogeneous lipid bilayers of 21 distinct lipid A types from 12 bacterial species are modeled and simulated to investigate the differences and similarities of their membrane properties such as the area per lipid, the hydrophobic thickness, and acyl chain order. In addition, different neutralizing ion types (Ca^{2+}, K^+, and Na^+) are considered to examine the ion's influence on the membrane properties including lipid diffusion coefficients, ion residence times, and compressibility modulus.

MATERIALS AND METHODS

Lipid A models, force field parameters, and initial structures

As shown in Table 1, 21 types of lipid A structures from 12 bacterial species were chosen and modeled based on the literature (Figs. 1 and S1 in the Supporting Material), but minor structural forms were not considered in this study.

Acinetobacter baumannii has recently been documented as a particularly threatening pathogenic bacterium because of its diverse infections in humans (5). *A. baumannii* lipid A has two major forms. Both types have the standard headgroup of the β-(1→6)-linked D-glucosamine (GlcN) disaccharide that is phosphorylated at 1- and 4′-positions, but differ with hepta- or hexa-acyl chains attached to the headgroup (6–8). In hepta-acylated lipid A, four primary acyl chains are linked to the disaccharide backbone in 2-, 3-, 2′-, and 3′-positions, and three secondary acyl chains are esterified to the hydroxyl groups of the 2-, 2′-, and 3′-primary acyl chains (Fig. 1; see Fig. S1 for the position numbers and acyl chain terminal carbon numbers),

TABLE 1   Lipid A Types and Systems in this Study

Bacteria	System	N_{CHAIN} [a]	$L_{\text{CHAIN}}^{\min}$ [a]	$L_{\text{CHAIN}}^{\max}$ [a]	Chemical Modification	Neutralizing ion Type
A. baumannii	AB-A	7	12	14		Ca^{2+}, K^+, Na^+
A. baumannii	AB-B	6	12	14		Ca^{2+}, K^+, Na^+
B. cepacia	BC-A	5	14	16		Ca^{2+}
B. pseudomallei	BC-B	5	14	16	1-P-β-L-Ara4N[b]	Ca^{2+}
C. jejuni	CJ-A	6	14	16	GlcN3N[c] as second sugar	Ca^{2+}
E. coli	EC-A	6	12	14		Ca^{2+}, K^+, Na^+
H. pylori	HP-A	4	16	18	1-PEtN and 4′-OH[d]	Ca^{2+}
H. pylori	HP-B	6	14	18		Ca^{2+}
K. pneumoniae	KP-A	7	14	16		Ca^{2+}
K. pneumoniae	KP-B	6	14	14		Ca^{2+}
N. gonorrheae	NG-A	6	12	14		Ca^{2+}
P. aeruginosa	PA-A	6	10	12		Ca^{2+}, K^+, Na^+
P. aeruginosa	PA-B	5	10	12		Ca^{2+}, K^+, Na^+
S. typhimurium	ST-A	7	12	16		Ca^{2+}
S. typhimurium	ST-B	7	12	16	1-, and 4′-P-β-L-Ara4N[e]	Ca^{2+}
S. typhimurium	ST-C	7	12	16	1-, and 4′-PPEtN[f]	Ca^{2+}
V. cholera	VC-A	6	12	14		Ca^{2+}
V. cholera	VC-B	6	12	14	3-Gly[g] on sixth chain	Ca^{2+}
V. cholera	VC-C	6	12	14	3-diGly[h] on sixth chain	Ca^{2+}
Y. pestis	YP-A	6	12	16		Ca^{2+}
Y. pestis	YP-B	4	14	14		Ca^{2+}

[a]N_{CHAIN}, $L_{\text{CHAIN}}^{\min}$, and $L_{\text{CHAIN}}^{\max}$ are the number of chains, the minimum chain length, and the maximum chain length in a given lipid A molecule, respectively.
[b]L-Ara4N is 4-amino-4-deoxy-L-arabinose and is attached to the 1-phosphate group.
[c]GlcN3N is 2,3-diamino-2,3-dideoxy-D-glucose and it replaces D-glucosamine (GlcN).
[d]1-PEtN and 4′-OH are the phosphoethanolamine and hydroxyl groups, and they replace the 1- and 4′-phosphate groups, respectively.
[e]L-Ara4N is 4-amino-4-deoxy-L-arabinose, and is attached to the 1- and 4′-phosphate groups.
[f]PPEtN is pyrophosphoethanolamine and it replaces the 1- and 4′-phosphate groups.
[g]Gly is glycine, and is attached to the C3′ position secondary acyl chain.
[h]diGly is diglycine, and is attached to the C3′ position secondary acyl chain.
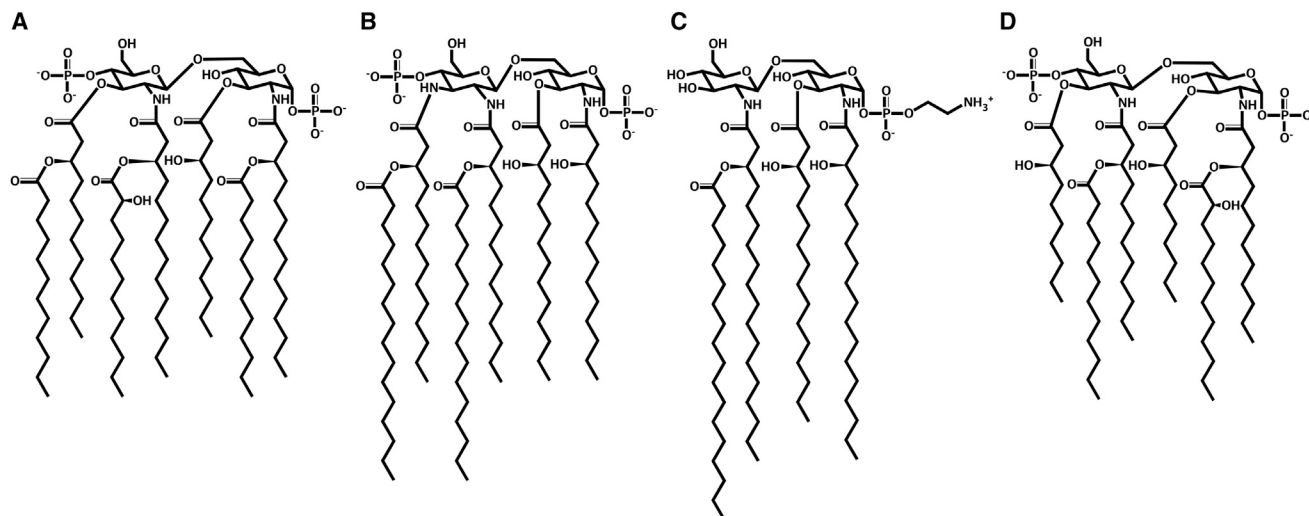
FIGURE 1   Selected lipid A chemical structures: (*A*) *A. baumannii*, (*B*) *C. jejuni*, (*C*) *H. pylori*, and (*D*) *P. aeruginosa*; see Fig. S1 for all lipid A structures in Table 1 with the position numbers and acyl chain terminal carbon numbers.

i.e., the C2 position contains a primary amide-linked C_{14}(3-OH, meaning a hydroxyl group attached to the C_3 position) and a secondary ester-linked C_{12}; the C3 position contains a primary ester-linked C_{12}(3-OH); the C-2′ position contains a primary amide-linked C_{14}(3-OH) and a secondary ester-linked C_{12}(2-OH); and the C3′ position contains a primary ester-linked C_{12}(3-OH) and a secondary ester-linked C_{12}. In hexa-acylated lipid A, a secondary acyl chain at the 2-primary acyl chain is missing. In this study, hepta- and hexa-acylated lipid A from *A. baumannii* are denoted as AB-A and AB-B, respectively.

Burkholderia cepacia has a lower virulence to humans than do other causative agents, and mostly infects plants (9). *B. cepacia* lipid A consists of the standard headgroup and five acyl chains. Four primary acyl chains are linked to the disaccharide backbone in the 2-, 3-, 2′-, and 3′-positions, and only the 2′-primary acyl chain has a secondary acyl chain (Fig. S1), i.e., C2 C_{16}(3-OH), C3 C_{14}(3-OH), C2′ C_{16}(3-OH) and a secondary ester-linked C_{14} and C3′ C_{14}(3-OH) (10,11).

Burkholderia pseudomallei is related to the outbreak of melioidosis, a contagious disease mainly found in tropical regions; recently, however, melioidosis has been spreading globally. The structure of *B. pseudomallei* lipid A has the same number of chains and length as *B. cepacia*, but 4-amino-4-deoxy-L-arabinose (Ara4N) is linked to the 1-phosphate group (12). In this study, lipid A from *B. cepacia* and *B. pseudomallei* are denoted as BC-A and BC-B, respectively.

Campylobacter jejuni is one of the most common causes for intestinal infection and diarrhea (13). *C. jejuni* lipid A consists of 1-, 4′-phosphorylated disaccharide with the β-(1→6)-linkage and six acyl chains. Unlike the other lipid A, as shown in Fig. 1, the terminal GlcN residue in *C. jejuni* lipid A is replaced with 3′-amino-3′-deoxy-D-glucosamine (GlcN3N). Four primary acyl chains are linked to the disaccharide in 2-, 3-, 2′-, and 3′-positions, and two secondary acyl chains are esterified to the hydroxyl groups of the 2′-, and 3′-primary acyl chains, i.e., C2 C_{14}(3-OH), C3 C_{14}(3-OH), C2′ C_{14}(3-OH) and a secondary ester-linked C_{16}, and C3′ C_{14}(3-OH) and a secondary ester-linked C_{16} (14,15). In this study, *C. jejuni* lipid A is denoted as CJ-A.

Escherichia coli's main concern to public health is gastrointestinal diseases (16). *E. coli* lipid A is made up of the standard headgroup and six acyl chains (Fig. S1). Four primary acyl chains are linked to sugar backbone in 2-, 3-, 2′-, and 3′-positions, and two secondary acyl chains are esterified to the hydroxyl groups of the 2′-, and 3′-primary acyl chains, i.e., C2 C_{14}(3-OH), C3 C_{14}(3-OH), C2′ C_{14}(3-OH) and a secondary ester-linked C_{12}, and the C3′ C_{14}(3-OH) and a secondary ester-linked C_{14} (17). In this study, *E. coli* lipid A is denoted as EC-A.

Helicobacter pylori is well adapted to the human gastrointestinal tract, and is responsible for illnesses such as chronic gastritis or gastric carcinoma (16,18). To evade the detection by the innate immune system, *H. pylori* generates two distinctive types of lipid A with tetra- and hexa-acyl chains. Tetra-acylated lipid A consists of the GlcN-containing disaccharide with β-(1→6)-linkage. As shown in Fig. 1, the only phosphate group on the 1-position in this lipid A is substituted by phosphoethanolamine (PEtN), giving net charge of zero for this lipid A. Due to the lack of the primary acyl chain on the 3′-position, three primary acyl chains are linked to the backbone in 2-, 3-, and 2′-positions, and only the 2′-primary acyl chain has a secondary acyl chain, i.e., C2 C_{18}(3-OH), C3 C_{16}(3-OH), C2′ C_{18}(3-OH), and a secondary ester-linked C_{18}. Hexa-acylated lipid A has the standard headgroup and the six acyl chains in the 2-, 3-, 2′-, and 3′-positions (Fig. S1), i.e., C2 C_{18}(3-OH), C3 C_{16}(3-OH), C2′ C_{18}(3-OH) and a secondary ester-linked C_{18}, and C3′ C_{16}(3-OH) and a secondary ester-linked C_{14} (19–21). In this study, the tetra- and the hexa-acylated forms are denoted as HP-A and HP-B, respectively.

Klebsiella pneumoniae is one of the opportunistic pathogens that causes nosocomial septicemia, bacteremia, and pneumonia (22,23). *K. pneumoniae* has two main lipid A types with the standard headgroup and hepta- or hexa-acyl chains (Fig. S1). In hepta-acylated lipid A, four primary acyl chains are directly linked to sugars in the 2-, 3-, 2′-, and 3′-positions. Three secondary acyl chains are ester-linked to the 2-, 3-, and 3′-primary acyl chains, i.e., C2 C_{14}(3-OH) and a secondary ester-linked C_{16}, C3 C_{14}(3-OH), C2′ C_{14}(3-OH) and a secondary ester-linked C_{14}, and C3′ C_{14}(3-OH) and a secondary ester-linked C_{14}. The hexa-acylated lipid A form is the same as the hepta-acylated form, but there is no secondary C_{16} in the 2-position (24,25). In this study, the hepta- and the hexa-acylated lipid A systems are denoted as KP-A and KP-B, respectively.

Neisseria gonorrheae is the causative agent responsible for gonorrhea, which is mostly transmitted through sexual contact (26,27). *N. gonorrheae* lipid A consists of the standard headgroup and six acyl chains. Four primary acyl chains are linked to the 2-, 3-, 2′-, and 3′-positions, and two secondary acyl chains are linked to the 2- and 2′-primary acyl chains (Fig. S1), i.e., C2 C_{14}(3-OH) and a secondary ester-linked C_{12}, C3 C_{12}(3-OH), C2′ C_{14}(3-OH), and a secondary ester-linked C_{12}, and C3′ C_{12}(3-OH) (28,29). In this study, *N. gonorrheae* lipid A is denoted as NG-A.

Pseudomonas aeruginosa is a common cause of Gram-negative infections, especially in immunocompromised patients, and can also aggravate congenital cystic fibrosis after birth (30). *P. aeruginosa* synthesizes two

major forms of hexa- and penta-acylated lipid A, which are grown in low-magnesium (8 μM) and high-magnesium (1 mM) conditions, respectively. As shown in Fig. 1, hexa-acylated lipid A is made up of the standard head-group and six acyl chains, i.e., C2 C_{12}(3-OH) and a secondary ester-linked C_{12}(2-OH), C3 C_{10}(3-OH), C2′ C_{12}(OH) and a secondary ester-linked C_{12}, and C3′ C_{10}(3-OH); presence of 2-OH at C2′ is discussed by Nikaido (31), but it is not considered in this study. In penta-acylated lipid A, there is no C3 C_{10}(3-OH) primary chain (Fig. S1) (30,32,33). In this study, the hexa- and the penta-acylated lipid A are denoted as PA-A and PA-B, respectively.

Salmonella typhimurium is mainly found in the intestinal lumen and is a common cause of gastroenteritis in humans (21). Usually, *S. typhimurium* lipid A is chemically modified in the final synthesis step with phospho-Ara4N or pyrophosphoethanolamine (PPEtN) in both phosphate groups, which gives rise to lipid A heterogeneity (34). The general form of unsubstituted *S. typhimurium* lipid A consists of the standard headgroup and seven acyl chains. Four primary acyl chains are linked to 2-, 3-, 2′-, and 3′-positions, and three secondary acyl chains are linked to 2-, 2′-, and 3′-primary acyl chains, i.e., C2 C14(3-OH) and a secondary ester-linked C16, C3 C14(3-OH), C2′ C14(3-OH), and a secondary ester-linked C12, and C3′ C14(3-OH) and a secondary ester-linked C14 (Fig. S1). Ara4N and PPEtN can be substituted on 1- and 4′-phosphate groups, respectively. In this study, the unsubstituted, Ara4N-substituted, and PEtN-substituted lipid A are denoted as ST-A, ST-B, and ST-C, respectively.

Vibrio cholerae is the causative agent of cholera, which is usually transmitted by unclean water and often causes severe diarrhea in humans and animals (35). *V. cholerae* lipid A consists of the standard headgroup and six acyl chains. Four primary acyl chains are linked to the 2-, 3-, 2′-, and 3′-positions, and two secondary acyl chains are linked to the 2′- and 3′-primary acyl chains, i.e., C2 C_{14}(3-OH); C3 C_{12}(3-OH); C2′ C_{14}(3-OH) and a secondary ester-linked C_{14}; and C3′ C_{12}(3-OH) and a secondary ester-linked C_{12} (Fig. S1), which is denoted as VC-A. Hankins et al. (35) reported the chemical modifications of a glycine or diglycine residue to the C3′ position secondary acyl chain, which are denoted as VC-B (glycine) and VC-C (diglycine), respectively.

Yersinia pestis holds historical significance as the pathogen responsible for the Medieval Black Death (36). The transmission of the epidemic occurred through infected, parasitic fleas on a mammalian host. The composition of *Y. pestis* lipid A is switched after transfer from flea to human because of the growth temperature (37). At a temperature of 21 °C, *Y. pestis* generates hexa-acylated lipid A. However, at a temperature of 37 °C, *Y. pestis* forms a tetra-acylated lipid A that allows undetected proliferation in the human body (38). Hexa-acylated lipid A has the standard headgroup, and four primary C_{14} acyl chains are linked to the 2-, 3-, 2′-, and 3′-positions, and two secondary acyl chains, as C_{12} and $C_{16:1}$, are linked to the 2′- and 3′-primary acyl chains (Fig. S1). In tetra-acylated lipid A, two secondary acyl chains are removed. In this study, hexa-acylated and tetra-acylated *Y. pestis* lipid A systems are denoted as YP-A and YP-B, respectively.

Simulation systems and protocols

We modeled homogeneous lipid A bilayers for 21 different lipid A types (Table 1) following the CHARMM-GUI *Membrane Builder* step-by-step protocol (39–41). The force-field parameters for each lipid A were assigned from the CHARMM36 force field for LPS (42), lipids (43), carbohydrates (44–46), and proteins (47). Each system contains 72 lipid A molecules (36 in each leaflet) with neutralizing Ca^{2+} ions in 150 mM KCl. To investigate the influence of ion types used to neutralize negatively charged lipid A molecules, five systems (AB-A, AB-B, EC-A, PA-A, and PA-B) were chosen and Ca^{2+} ions were replaced by K^+ or Na^+ ions (48,49) that were placed near lipid A (Table 1). The number of atoms in each system are ~57,000. Three replicas for each bilayer system were built to improve sampling and to check simulation convergence.

The equilibration and production of all systems also followed the CHARMM-GUI *Membrane Builder* procedure (50). All systems were equilibrated for 450 ps by gradually reducing various restraint force constants using CHARMM (51). At the beginning of equilibration, a 1-fs time step Langevin dynamics was used and changed to a 2-fs time step for constant particle number, pressure, and temperature (NPT) dynamics. The SHAKE algorithm (52) was used to constrain the bond lengths involving hydrogen atoms. After an additional 10-ns equilibration run using CHARMM, an NPT production run was followed for 250 ns (K^+ and Na^+ systems) or 350 ns (Ca^{2+} systems) using NAMD (53) at 310.15 K and 1 bar, respectively. The van der Waals interactions were smoothly switched to zero over 10–12 Å by the force-based switching function (54), and the particle mesh Ewald method was used to calculate the long-range electrostatic interactions (55). Nosé-Hoover Langevin piston control (56,57) was used for constant pressure with 50 fs piston period and 25 fs piston decay time, and Langevin dynamics was used for constant temperature with a 1 ps^{-1} Langevin coupling coefficient. The dihedral angle restraints for sugar rings were applied to keep appropriate chair conformations and were maintained during the production simulations.

Nonbonded interaction FIX parameters and their effects on membrane properties

The nonbonded interaction FIX (NBFIX) term in the CHARMM force field parameter set can be employed to use different van der Waals interactions between specific atom pairs instead of atom type-based generic Lennard-Jones parameters (48,49). When the original Ca^{2+} parameters were used, a few systems including the AB-B model showed acute angles between the O6-C2 (in GlcN) vector and the O6-C4′ (in GlcN′) vector because of too tight binding between Ca^{2+} and phosphate oxygen atoms in Lipid A (Fig. S2 A). For example, ~25% of AB-A molecules had such acute angles. Note that our previous *E. coli* simulations (58–60) (including EC-A in this study) did not show this behavior. When the NBFIX parameters in Fig. S2 B (recently optimized by B. Roux and S. Rong, personal communication) were used, the number of such abnormal structure forms (i.e., acute angles) disappeared. For example, in AB-B systems, when the NBFIX parameters were applied at 150 ns, such tight binding between Ca^{2+} ions and lipid A disappeared after 400 ns (Fig. S2 C). The area per lipid (APL) and the hydrophobic thickness (T_{MEMB}), in which T_{MEMB} is defined by the average z values between the carbon atoms after carbonyl groups in the upper and lower leaflets, were converged along the simulation. Because these simulations with NBFIX applied at 150 ns required long reequilibration, we ran all the simulations with the NBFIX parameters from the beginning for 350 ns (as stated above) and all the results (except the pressure profiles) are based on these simulations.

RESULTS AND DISCUSSION

The bilayer properties of lipid A from various Gram-negative bacteria (Table 1) are characterized by APL, T_{MEMB}, and the acyl chain order parameters ($|S_{CD}|$) calculated over the last 200 ns trajectory of each lipid A system (average and standard errors over three replicates). We first describe these properties for the systems with neutralizing Ca^{2+} ions in the context of variations in N_{CHAIN}, L_{CHAIN}, and chemical modifications to the standard 1-, 4′-phosphorylated lipid A form. Then, the influence of K^+ or Na^+ ions (as different neutralizing ions) on these properties as well as lipid diffusion coefficients, ion residence times, and compressibility modulus is described. Finally, a distinctive characteristic of the pressure profile of lipid A bilayers is presented and discussed.

Bilayer properties of various lipid A with neutralizing Ca^{2+} ions

Fig. 2 A shows the APL of each lipid A containing the standard 1-, 4′-phosphorylated disaccharide. Clearly, a linear relation is observed between the APL and N_{CHAIN}; as N_{CHAIN} increases, the APL increases with small variations within the same N_{CHAIN} (Fig. 2 B). To find better correlations including L_{CHAIN}, two different average values of L_{CHAIN} are considered because the length of each acyl chain in different lipid A is variable. The first one ($\langle L_{CHAIN} \rangle_1$ in Fig. 2 D) is a simple average (i.e., the total number of acyl chain carbon atoms divided by N_{CHAIN}) and the second one ($\langle L_{CHAIN} \rangle_2$ in Fig. 2 D) considers the position of (secondary) 3-O acyl chain(s), so that the average is taken after adding +3 to such secondary acyl chain length. In the same N_{CHAIN} systems, the APL decreases as L_{CHAIN} increases, which is consistent with the previous studies on phospholipids (61). In linear least squares regression scheme, as shown in Fig. 3 A, the APL is best described by

$$APL = 13.78 \times N_{CHAIN} - 1.03 \times \langle L_{CHAIN} \rangle_2 - 94.34. \quad (1)$$

In addition, we have tried to fit APL using a polymer brush model (PBM), but the result could not capture the decrease in APL with increasing L_{CHAIN} for the lipid A molecules with the same N_{CHAIN} (the PBM used in this work is described in detail in the Supporting Material). We attribute this to the absence of the van der Waals interactions in the PBM (62). While Eq. 1 is empirical and does not have any physical meaning, it is expected that the APL of an unknown lipid A type can be estimated by this equation to set up an initial membrane system (63). Snyder et al. (64) estimated the APL/N_{CHAIN} to be ~26 $Å^2$ for liquid-crystalline bilayer structures of LPS from *Salmonella minnesota* and *S. typhimurium*. The experimental values appear to fit with our simulation data for lipid A systems containing six or seven chains with a range of 25.2–27.3 $Å^2$ (Fig. 2 B). Interestingly, the APL/N_{CHAIN} increases as N_{CHAIN} decreases, indicating that lipid A acyl chains are packed tighter with larger N_{CHAIN}.

Fig. 2 C shows T_{MEMB} of each lipid A containing the standard 1-, 4′-phosphorylated disaccharide. T_{MEMB} is generally correlated with $\langle L_{CHAIN} \rangle_2$, but there are also some contributions from N_{CHAIN}. In linear regression, as shown in Fig. 3 B, T_{MEMB} is best described by

$$T_{MEMB} = 2.26 \times \langle L_{CHAIN} \rangle_2 + 1.20 \times N_{CHAIN} - 16.56. \quad (2)$$

Similar to Eq. 1, the T_{MEMB} (i.e., z position) of an unknown lipid A type can be estimated by Eq. 2 and used to set up an initial membrane system.
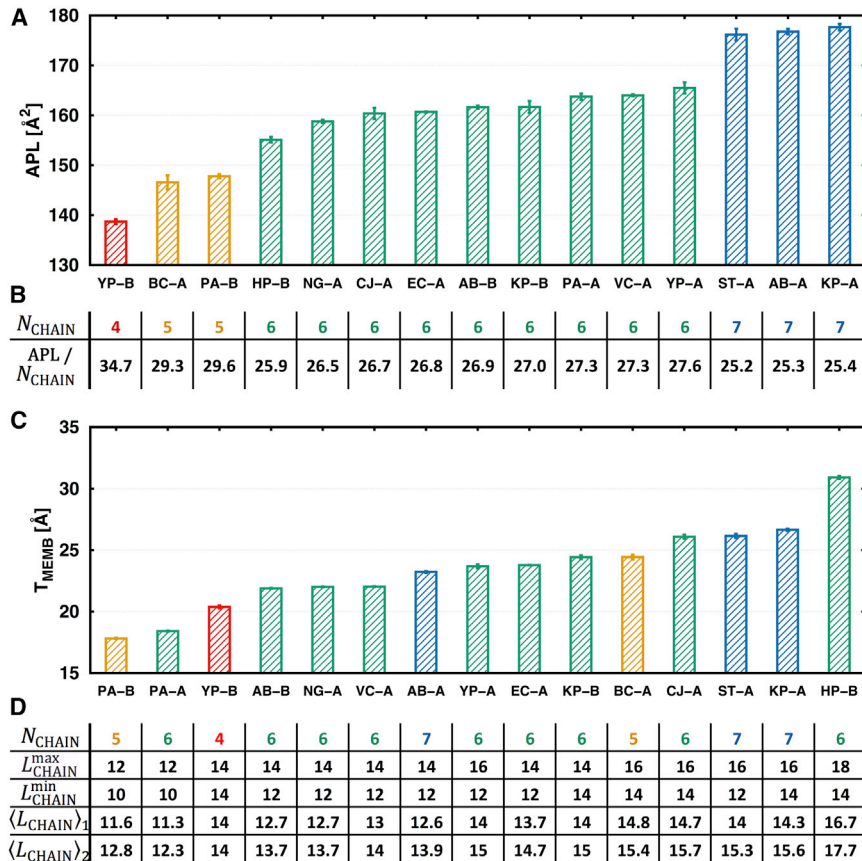

A

B

N_{CHAIN}	4	5	5	6	6	6	6	6	6	6	6	6	7	7	7
APL / N_{CHAIN}	34.7	29.3	29.6	25.9	26.5	26.7	26.8	26.9	27.0	27.3	27.3	27.6	25.2	25.3	25.4

C

D

N_{CHAIN}	5	6	4	6	6	6	7	6	6	6	5	6	7	7	6
L_{CHAIN}^{max}	12	12	14	14	14	14	14	16	14	14	16	16	16	16	18
L_{CHAIN}^{min}	10	10	14	12	12	12	12	12	12	14	14	14	12	14	14
$\langle L_{CHAIN} \rangle_1$	11.6	11.3	14	12.7	12.7	13	12.6	14	13.7	14	14.8	14.7	14	14.3	16.7
$\langle L_{CHAIN} \rangle_2$	12.8	12.3	14	13.7	13.7	14	13.9	15	14.7	15	15.4	15.7	15.3	15.6	17.7

FIGURE 2 (A) APL and (C) T_{MEMB} of 1-, 4′-phosphorylated lipid A with the standard errors over three replicas. (B) APL/L_{CHAIN} of each lipid A system in the order of (A). (D) L_{CHAIN}^{min}, L_{CHAIN}^{max}, $\langle L_{CHAIN} \rangle_1$, and $\langle L_{CHAIN} \rangle_2$ of each lipid A system in the order of (C). $\langle L_{CHAIN} \rangle_1$ and $\langle L_{CHAIN} \rangle_2$ are the average L_{CHAIN} with different weight schemes (see the main text). To see this figure in color, go online.
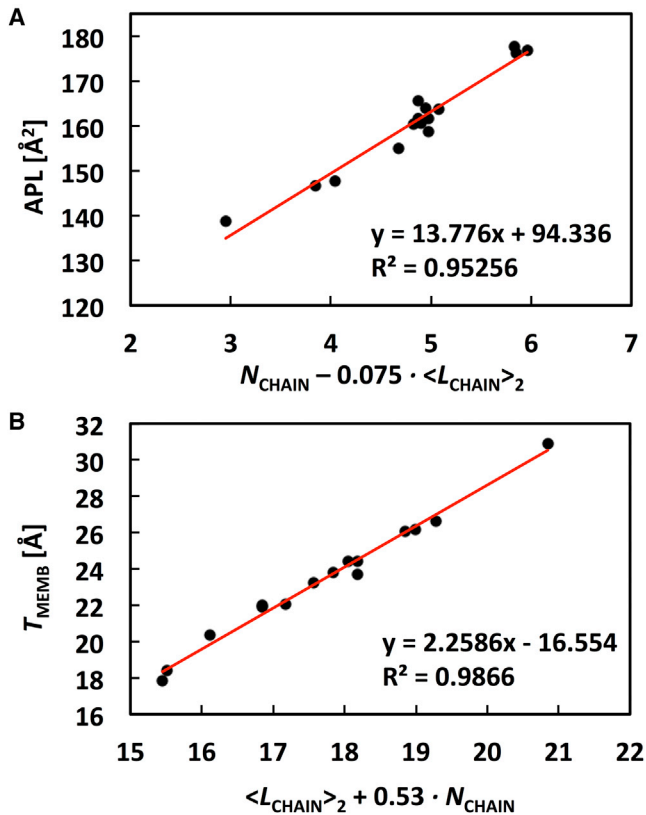
FIGURE 3 Correlation (*A*) between APL and $[N_{CHAIN} - 0.075 \times \langle L_{CHAIN} \rangle_2]$ and (*B*) between T_{MEMB} and $[\langle L_{CHAIN} \rangle_2 + 0.53 \times N_{CHAIN}]$. To see this figure in color, go online.

FIGURE 4   (*A*) APL and (*B*) T_{MEMB} of the eight chemically modified lipid A bilayers. To see this figure in color, go online.

To investigate the effects of various chemical modifications on APL and T_{MEMB}, eight lipid A systems are compared (L-Ara4N in BC-B and ST-B, PEtN in ST-C, Gly in VC-B, and diGly in VC-C; see Table 1). In our simulation, the effect of L-Ara4N and PEtN on APL and T_{MEMB} is not observed (Figs. 4, *A* and *B*) because L-Ara4N and PEtN are located above the disaccharide (Figs. S3, *A* and *B*). In the case of Gly and diGly substitution to the O-3 secondary acyl chain, the membrane properties are highly affected. During the simulations, both Gly and diGly residues moved toward the lipid A headgroup (Figs. S3, *C* and *D*) and interacted with inter- or intraphosphate groups (Figs. S3, *E* and *F*), so the linked acyl chains were disordered. In addition, Gly and diGly occupy a certain physical volume, which makes lipid A less packed and thus, the APL values larger.

To check the correlation between $|S_{CD}|$ and the APL (and T_{MEMB}), two systems, i.e., PA-A and HP-B, are considered as both have six acyl chains. As shown in Fig. 5 *A*, the membrane properties are very distinguishable as they have different L_{CHAIN}. The short chains in PA-A become more disordered (i.e., lower $|S_{CD}|$ in Fig. 5 *B*), which results in decreased T_{MEMB} and increased APL. In contrast, the long chains in HP-B show the opposite trend (Figs. 5, *A* and *C*). *H. pylori* has two types of lipid A that have different
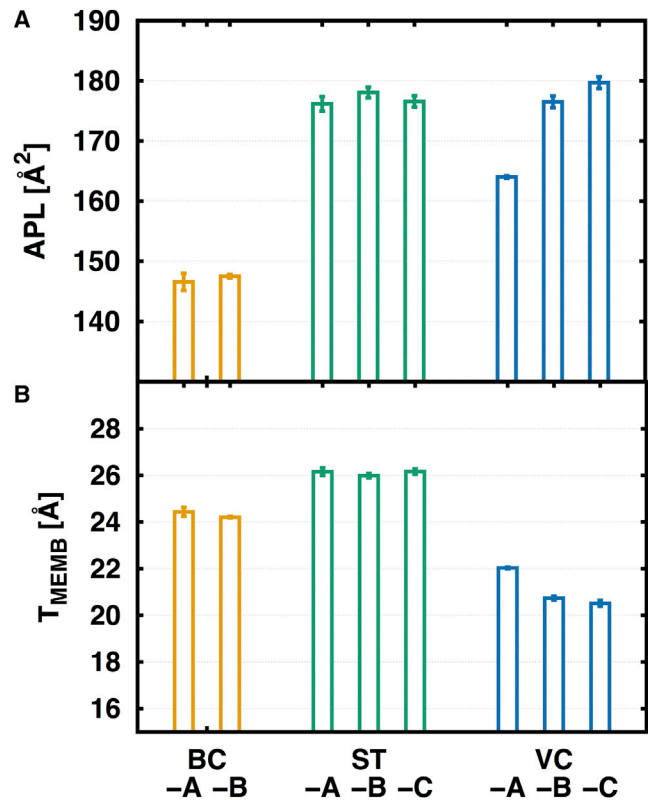
N_{CHAIN} (4 for HP-A and 6 for HP-B). In particular, tetra-acylated HP-A has 1-PEtN and 4′-OH substitutions to evade detection by the cationic antimicrobial peptide and Toll-like receptor 4 (21). As shown in Fig. 5 *A*, the main difference in their APL arises from different N_{CHAIN}, and APL/N_{CHAIN} are 25.03 Å^2 (HP-A) and 25.85 Å^2 (HP-B), which are on the smaller side compared to other lipid A systems due to large $\langle L_{CHAIN} \rangle_2$ (Table S1). Clearly, as indicated by APL and T_{MEMB}, HP-A molecules are slightly better packed and have higher $|S_{CD}|$ than HP-B. While the $|S_{CD}|$ value is high in both HP-A and HP-B, the lipid A bilayers are still in a liquid-disordered phase.

The lipid A disaccharide's glycosidic torsion angle distributions from the last 200 ns simulation of AB-A are shown in Fig. S4 *A*. To compare the results with those from x-ray structures, 27 lipid A structures from 18 Protein Data Bank IDs were collected and the glycosidic torsion angles were measured. Our simulation model and x-ray structures show good agreement; 80% of lipid A x-ray structures are overlapped with simulation torsion angle distribution. Also, all other systems show very similar glycosidic torsion angle distributions (Figs. S4, *A* and *B*; other data not shown), indicating that the disaccharide conformations of lipid A molecules studied in this work are not affected by N_{CHAIN}, L_{CHAIN}, and chemical modifications.
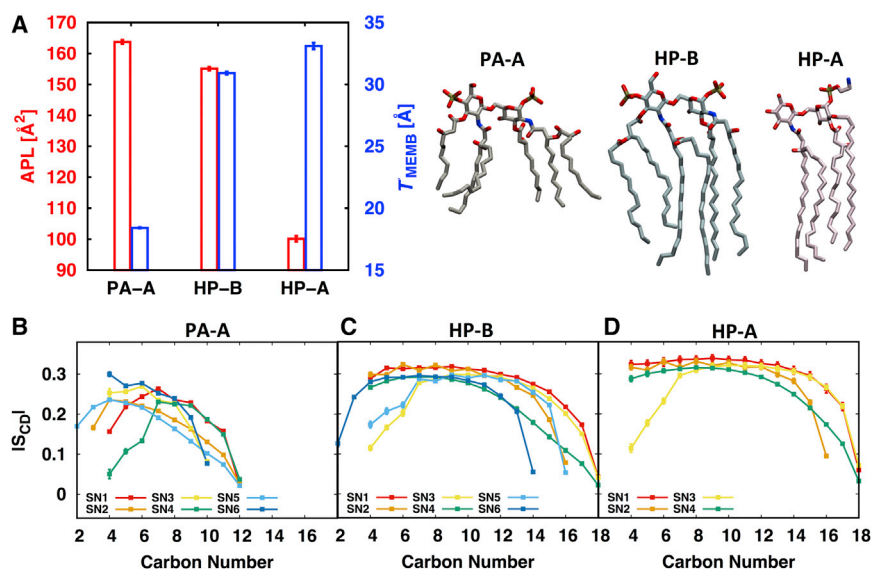
FIGURE 5 (A) APL and T_{MEMB} of PA-A, HP-B, and HP-A with the representative lipid A structure. $|S_{CD}|$ of each acyl chain for (B) PA-A, (C) HP-B, and (D) HP-A. To see this figure in color, go online.

Influence of neutralizing ion types on bilayer properties

It is known that divalent cations play an important role in stabilization of the outer membrane; Mg^{2+} and Ca^{2+} ions chelate and neutralize the repulsion between adjacent LPS (58,65–67). In this simulation, the Ca^{2+} ions were used as divalent cation to neutralize negatively charged lipid A simply due to the fact that the Ca^{2+} force field is better parameterized than Mg^{2+}. To investigate the influence of neutralizing ion types on bilayer properties, five bilayer systems (AB-A, AB-B, EC-A, PA-A, and PA-B; see Table 1) were chosen and Ca^{2+} ions were replaced by K^+ or Na^+ ions. The analysis indicates that neutralizing ion types show minimal effects on bilayer properties such as APL and T_{MEMB}. As the ion type changes from Ca^{2+} to K^+ or Na^+, the APL values are slightly decreased and T_{MEMB} values are mostly similar or slightly increased (Fig. 6). Clearly, all the cations can stabilize the lipid A bilayer.

The thermal movement of lipid bilayers can be characterized with lateral diffusion coefficients of lipids in the membrane plane. The diffusion coefficients of lipid A (D_L) were estimated from the slope of the two-dimensional lateral mean square displacement (MSD): $D_L = \lim_{t \to \infty} d\langle|\mathbf{r}(t+t_0) - \mathbf{r}(t_0)|^2\rangle_{t_0}/4dt$, where $\mathbf{r}$ is the displacement vector of the center of mass of lipid A, t_0 is the time origin for MSD calculations ranging from $t_{max} - t$ to t_{max}, and t_{max} is the total simulation time. The MSD was calculated for all lipid A molecules after removal of the leaflet drift (Fig. S5 A), and its linear region (40–100 ns) was used to estimate D_L. The Ca^{2+} neutralized systems showed the D_L of 0.70–1.01 μm^2/s (Table 2), which is ~10 times slower than phospholipids in their bilayers (68). The D_L in K^+ and Na^+ neutralized systems were

1.20–2.35 μm^2/s and 0.98–1.48 μm^2/s, respectively. Clearly, the lipid A mobility decreases in the presence of Ca^{2+}, and agrees with the experimental estimates with LPS diffusion coefficients (~1 μm^2/s) (69).
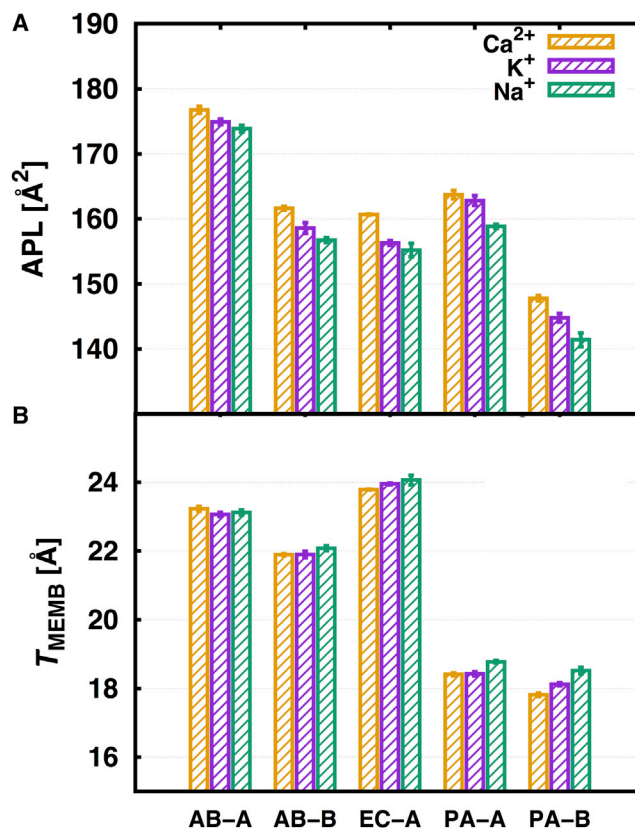

FIGURE 6 (A) Results of APL and (B) T_{MEMB} on different neutralizing ion types with color as yellow, Ca^{2+}; purple, K^+; and green, Na^+. To see this figure in color, go online.

TABLE 2 Diffusion Coefficients, Residence Times, and Compressibility Modulus of the Five Lipid A Systems with Three Different Neutralizing Ion Types and the Standard Errors over Three Replicates

Neutralizing ion	System	Diffusion Coefficient (μm^2/s)	Residence Time of Ion (ns)	Compressibility Modulus (dyn/cm)
Ca^{2+}	AB-A	0.75 ± 0.07	73 ± 14	46 ± 8
	AB-B	1.01 ± 0.07	64 ± 1	40 ± 3
	EC-A	0.96 ± 0.12	68 ± 11	33 ± 9
	PA-A	0.99 ± 0.11	67 ± 10	47 ± 13
	PA-B	0.70 ± 0.16	92 ± 8	47 ± 5
K^+	AB-A	2.35 ± 0.26	4 ± 1	15 ± 3
	AB-B	1.75 ± 0.25	7 ± 1	27 ± 1
	EC-A	1.20 ± 0.13	8 ± 0	24 ± 6
	PA-A	2.28 ± 0.52	8 ± 1	26 ± 5
	PA-B	2.12 ± 0.20	10 ± 1	29 ± 6
Na^+	AB-A	1.48 ± 0.31	19 ± 2	17 ± 3
	AB-B	0.98 ± 0.16	24 ± 2	32 ± 8
	EC-A	1.08 ± 0.20	28 ± 1	26 ± 4
	PA-A	1.47 ± 0.12	24 ± 1	19 ± 4
	PA-B	1.06 ± 0.15	33 ± 2	38 ± 1

To understand the contact between neutralizing ions and lipid A molecules, the residence time was measured based on the method by Impey et al. (70), which has been adopted to calculate the intermolecular contact as a function of time. The function $P_{ij}(t_0,t_0 + t; t^*)$ is set to 1 if the neutralizing ion and the lipid A phosphate group are within the cutoff distance (4.5 Å) between t_0 and $t_0 + t$ without separation longer than a tolerance time ($t^* = 20$ ps), or 0 otherwise. The average number of the contact at time t is defined as $n(t) = \sum_{t_0=1}^{t_{max}-t}\sum_{i=1}^{N_I}\sum_{j=1}^{N_L}P_{ij}(t_0,t_0+t;t^*)/(t_{max} - t)$, where N_I and N_L are the numbers of neutralizing ions and lipid A, and t_{max} is a total simulation time (Fig. S5 B). The mean residence time of ions (τ_{ion}) can be estimated by fitting $n(t)$ to $\exp(-t / \tau_{ion})$ at large t. It is known that the residence times decrease as the ion size increases ($\tau_{Na} > \tau_K$) (70), and the divalent ion showed larger τ_{ion} than the monovalent ion (71). Similar to these results, in our simulation results, Ca^{2+} ions (46–87 ns) dwelt on the membrane surface longer than Na^+ (16–28 ns), and K^+ ions (3–10 ns) exchanged quicker than Na^+ ions (Table 2). Clearly, Ca^{2+} ions stay on the lipid A membrane and stabilize the lipid A better than monovalent ions.

The compressibility modulus contains information on membrane packing, and can be calculated by $K_A = k_B T \, \text{APL}/(N\langle\delta\text{APL}^2\rangle)$, where $k_B T$ is the thermal energy and N is the number of lipid A systems in a leaflet. Cañadas et al. (72) showed that the K_A of typical phospholipid monolayers decrease with increasing LPS ratio and approaches to ~29 dyn/cm at the LPS molar fraction of 1 in buffer (5 mM Tris-HCl, 150 mM NaCl, 150 μM $CaCl_2$). In our simulation results, the K_A in the Ca^{2+} neutralized systems are 33–47 dyn/cm. In K^+ and Na^+ neutralized systems, the K_A are 15–29 dyn/cm and 17–38 dyn/cm, respectively; this suggests that the lipid A with monovalent cations (K^+ or Na^+) are more compressible than Ca^{2+} neutralized lipid A.

Correlation between chemical modification and membrane integrity

The effects of various chemical modifications on membrane integrity were investigated by comparing the diffusion coefficient, the Ca^{2+} ion residence time, and the compressibility for six lipid A systems (ST-A/B/C, and VC-A/B/C). As shown in Table S2, the effects of chemical modifications were not significant, and thus it can be considered that these chemical modifications do not perturb the membrane integrity significantly at the level of lipid A.

Distinctive characteristics of the lateral pressure profile

The lateral pressure of a bilayer is related to the surface tension, the curvature, and the behavior of membrane proteins (73–75). Generally, a membrane pressure profile along the z axis is not uniform because of the large interfacial free energy over membrane headgroups and water molecules; positive lateral pressure arises from repulsive interactions and negative pressure indicates attractive interactions. The lateral pressure profile is defined as $p(z) = p_L(z) - p_N(z)$, where $p_L(z) = [p_{xx}(z) + p_{yy}(z)]/2$ and $p_N(z) = p_{zz}(z)$ are the lateral and normal components of the pressure tensor, respectively. To calculate the lateral pressure profile, the long 1050 ns NAMD production run for the AB-B systems (see Materials and Methods) was used. The pressure profile was calculated using the Harasima contour (76) whose $p_N(z)$ cannot be simply obtained (77). Therefore, it was estimated as $p_N(z) = L_z^{-1} \int_{-L_z/2}^{L_z/2} dz \, p_L(z)$, where L_z is the box size along the z direction, under the assumption of a vanishing bilayer surface tension and the mechanical equilibrium (uniform p_N). The trajectories were saved at every 10 ps with the lateral pressure profile calculation along the z axis (0.5 Å for slab size), and the last 350 ns of data were used for the analysis. As the bilayer moved along
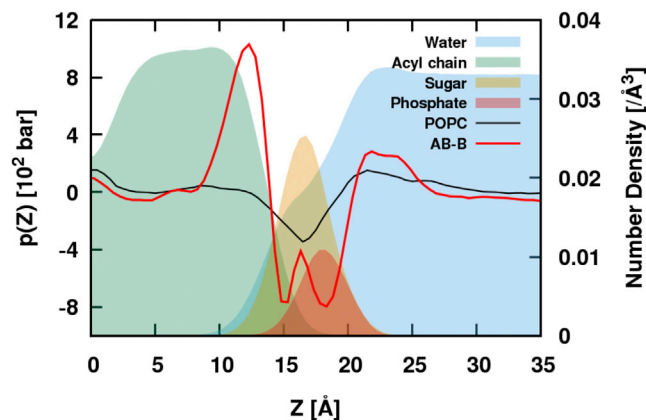
FIGURE 7 Lateral pressure profile of AB-B (*red line*) and POPC (*black line*) bilayers with the lateral density profiles (*solid layers*) of AB-B system with sky-blue for water, green for acyl tail, orange for disaccharide, and red for phosphate. Note that, as the magnitude of the lateral pressure depends on the system size, its variation along the z axis is the important feature. To see this figure in color, go online.

the z axis in the NAMD production run, every frame was re-centered to place the bilayer center at $z = 0$ by estimating the bilayer center (78). As the lipid A bilayer is homogeneous, the pressure profile results were symmetrized. In a pure POPC bilayer system (78), the headgroup region ($z = 13$–20 Å) yields negative pressure (Fig. 7), and this attraction dip begins with water-headgroup interfaces. In AB-B system, a double dip is observed in the interfacial region. A small peak inside the dip corresponds to the maximum peak of the disaccharide density along the z axis (Fig. 7). A large positive pressure is observed toward the bilayer center starting from the beginning of acyl chain, which appears to arise from the steric repulsion between acyl chains attached to the disaccharide. The bilayer leaflet curvature can be inferred from the first moment of the pressure profile: $\overline{F}' = -\int_0^\infty dz\, zp(z) = -k_c R_0^{-1}$ (75,76), where k_c (> 0) is the bending modulus and R_0^{-1} is the spontaneous curvature of the leaflet. The calculated $\overline{F}'$ for AB-B is 0.164 kcal/(mol·Å), implying that AB-B lipid A would induce negative curvature to the leaflet where it resides (if the constraints of the periodic boundary conditions are relaxed). This result is consistent with the work of Mingeot-Leclercq and Decout (79) in that LPS entices negative curvature strain and tends to adopt structures as inverted micelles or hexagonal phases. Note that the effects of different lipid A systems on the curvature of membrane may vary depending on the number of acyl chains and chemical modifications.

CONCLUSIONS

We have investigated the bilayer properties of 21 distinct lipid A types from 12 bacterial species and the influences of neutralizing ion types on the properties in terms of APL, membrane hydrophobic thickness (T_{MEMB}), and order

parameters ($|S_{CD}|$), lipid diffusion coefficients, ion residence times, and compressibility modulus using all-atom molecular dynamics simulations. The acyl chain number (N_{CHAIN}) and acyl chain length (L_{CHAIN}) play major roles in defining the bilayer properties. The N_{CHAIN} is correlated to the APL; the APL increases as a function of N_{CHAIN}. The APL/N_{CHAIN} increases as N_{CHAIN} decreases; lipid A acyl chains are better packed with higher N_{CHAIN}. The T_{MEMB} is mainly determined by $\langle L_{CHAIN} \rangle_2$, which is taken after adding $+3$ to secondary acyl chain length. Both APL and T_{MEMB} are not affected by the chemical modification of the 1-P and 4′-P positions to P-L-Ara4N and PPEtN. In the case of Gly and diGly substitution to O-3 secondary acyl chain, however, the membrane properties are highly affected. A good correlation among APL, T_{MEMB}, and $|S_{CD}|$ are observed; as APL increases, $|S_{CD}|$ decreases, and highly ordered lipid A has a larger T_{MEMB}. The influences of neutralizing ion types such as Ca^{2+}, K^+, and Na^+ on bilayer properties such as APL and T_{MEMB} are minimal, but the Ca^{2+} neutralized systems show the same trend in experiments in terms of lipid diffusion and lipid compressibility; Ca^{2+} ions reside longer on the lipid A headgroups than K^+ and Na^+ ion types, reducing lipid A lateral diffusion and inducing high lipid A compressibility. Thus, the resulting characteristics of different Lipid A obtained in this study form a basis toward the modeling and simulation of the outer membranes (with and without outer membrane proteins) of various Gram-negative bacteria. In particular, all lipid A models in this study are available through *LPS Modeler* in CHARMM-GUI, so that these models can be used to further our understanding of the structure, dynamics, and function of various bacterial outer membranes.

SUPPORTING MATERIAL

AUTHOR CONTRIBUTIONS

S.K. and W.I. designed the research; S.K., D.S.P., G.W., and W.I. performed the research; S.K., D.S.P., S.P., J.S., J.B.K., G.W., and W.I. analyzed the data; and S.K., D.S.P., S.P., J.S., J.B.K., G.W., and W.I. wrote the article.

ACKNOWLEDGMENTS

REFERENCES

1. Thomson, J. M., and R. A. Bonomo. 2005. The threat of antibiotic resistance in Gram-negative pathogenic bacteria: β-lactams in peril! *Curr. Opin. Microbiol.* 8:518–524.

2. Silhavy, T. J., D. Kahne, and S. Walker. 2010. The bacterial cell envelope. *Cold Spring Harb. Perspect. Biol.* 2:a000414.

3. Gessmann, D., Y. H. Chung, …, K. G. Fleming. 2014. Outer membrane β-barrel protein folding is physically controlled by periplasmic lipid head groups and BamA. *Proc. Natl. Acad. Sci. USA.* 111:5878–5883.

4. Fontana, C., R. Conde-Álvarez, …, G. Widmalm. 2016. Structural studies of lipopolysaccharide-defective mutants from *Brucella melitensis* identify a core oligosaccharide critical in virulence. *J. Biol. Chem.* 291:7727–7741.

5. Peleg, A. Y., H. Seifert, and D. L. Paterson. 2008. *Acinetobacter baumannii*: emergence of a successful pathogen. *Clin. Microbiol. Rev.* 21:538–582.

6. Fregolino, E., G. Fugazza, …, C. De Castro. 2010. Complete lipooligosaccharide structure of the clinical isolate *Acinetobacter baumannii*, strain SMAL. *Eur. J. Org. Chem.* 2010:1345–1352.

7. Pelletier, M. R., L. G. Casella, …, R. K. Ernst. 2013. Unique structural modifications are present in the lipopolysaccharide from colistin-resistant strains of *Acinetobacter baumannii*. *Antimicrob. Agents Chemother.* 57:4831–4840.

8. Sweet, C. R., G. M. Alpuche, …, B. C. Sandman. 2014. Endotoxin structures in the psychrophiles *Psychromonas marina* and *Psychrobacter cryohalolentis* contain distinctive acyl features. *Mar. Drugs.* 12:4126–4147.

9. Mahenthiralingam, E., T. A. Urban, and J. B. Goldberg. 2005. The multifarious, multireplicon *Burkholderia cepacia* complex. *Nat. Rev. Microbiol.* 3:144–156.

10. Ieranò, T., P. Cescutti, …, A. Molinaro. 2010. The lipid A of *Burkholderia multivorans* C1576 smooth-type lipopolysaccharide and its proinflammatory activity in a cystic fibrosis airways model. *Innate Immun.* 16:354–365.

11. Madala, N. E., M. R. Leone, …, I. A. Dubery. 2011. Deciphering the structural and biological properties of the lipid A moiety of lipopolysaccharides from *Burkholderia cepacia* strain ASP B 2D, in *Arabidopsis thaliana*. *Glycobiology.* 21:184–194.

12. Novem, V., G. Shui, …, G. Tan. 2009. Structural and biological diversity of lipopolysaccharides from *Burkholderia pseudomallei* and *Burkholderia thailandensis*. *Clin. Vaccine Immunol.* 16:1420–1428.

13. Guerry, P., C. M. Szymanski, …, A. P. Moran. 2002. Phase variation of *Campylobacter jejuni* 81–176 lipooligosaccharide affects ganglioside mimicry and invasiveness in vitro. *Infect. Immun.* 70:787–793.

14. Wilkinson, S. G. 1996. Bacterial lipopolysaccharides—themes and variations. *Prog. Lipid Res.* 35:283–343.

15. Moran, A. P. 1997. Structure and conserved characteristics of *Campylobacter jejuni* lipopolysaccharides. *J. Infect. Dis.* 176 (*Suppl 2*):S115–S121.

16. Erridge, C., E. Bennett-Guerrero, and I. R. Poxton. 2002. Structure and function of lipopolysaccharides. *Microbes Infect.* 4:837–851.

17. Galanos, C., O. Lüderitz…, 1985. Synthetic and natural *Escherichia coli* free lipid A express identical endotoxic activities. *Eur. J. Biochem.* 148:1–5.

18. Parsonnet, J., G. D. Friedman, …, R. K. Sibley. 1991. *Helicobacter pylori* infection and the risk of gastric carcinoma. *N. Engl. J. Med.* 325:1127–1131.

19. Stead, C. M., A. Beasley, …, M. S. Trent. 2008. Deciphering the unusual acylation pattern of *Helicobacter pylori* lipid A. *J. Bacteriol.* 190:7012–7021.

20. Cullen, T. W., D. K. Giles, …, M. S. Trent. 2011. *Helicobacter pylori* versus the host: remodeling of the bacterial outer membrane is required for survival in the gastric mucosa. *PLoS Pathog.* 7:e1002454.

21. Needham, B. D., and M. S. Trent. 2013. Fortifying the barrier: the impact of lipid A remodelling on bacterial pathogenesis. *Nat. Rev. Microbiol.* 11:467–481.

22. Hansen, D. S., F. Mestre, …, V. J. Benedí. 1999. *Klebsiella pneumoniae* lipopolysaccharide O typing: revision of prototype strains and O-group distribution among clinical isolates from different sources and countries. *J. Clin. Microbiol.* 37:56–62.

23. Neuhauser, M. M., R. A. Weinstein, …, J. P. Quinn. 2003. Antibiotic resistance among Gram-negative bacilli in US intensive care units: implications for fluoroquinolone use. *JAMA.* 289:885–888.

24. Helander, I. M., Y. Kato, …, T. Yokochi. 1996. Characterization of lipopolysaccharides of polymyxin-resistant and polymyxin-sensitive *Klebsiella pneumoniae* O3. *Eur. J. Biochem.* 237:272–278.

25. Clements, A., D. Tull, …, R. A. Strugnell. 2007. Secondary acylation of *Klebsiella pneumoniae* lipopolysaccharide contributes to sensitivity to antibacterial peptides. *J. Biol. Chem.* 282:15569–15577.

26. Apicella, M. A., M. Ketterer, …, M. S. Blake. 1996. The pathogenesis of gonococcal urethritis in men: confocal and immunoelectron microscopic analysis of urethral exudates from men infected with *Neisseria gonorrhoeae*. *J. Infect. Dis.* 173:636–646.

27. Edwards, J. L., J. Q. Shao, …, M. A. Apicella. 2000. *Neisseria gonorrhoeae* elicits membrane ruffling and cytoskeletal rearrangements upon infection of primary human endocervical and ectocervical cells. *Infect. Immun.* 68:5354–5363.

28. Ellis, C. D., B. Lindner, …, R. Demarco de Hormaeche. 2001. The *Neisseria gonorrhoeae* lpxLII gene encodes for a late-functioning lauroyl acyl transferase, and a null mutation within the gene has a significant effect on the induction of acute inflammatory responses. *Mol. Microbiol.* 42:167–181.

29. Post, D. M. B., N. J. Phillips, …, M. A. Apicella. 2002. Intracellular survival of *Neisseria gonorrhoeae* in male urethral epithelial cells: importance of a hexaacyl lipid A. *Infect. Immun.* 70:909–920.

30. Ernst, R. K., E. C. Yi, …, S. I. Miller. 1999. Specific lipopolysaccharide found in cystic fibrosis airway *Pseudomonas aeruginosa*. *Science.* 286:1561–1565.

31. Nikaido, H. 2003. Molecular basis of bacterial outer membrane permeability revisited. *Microbiol. Mol. Biol. Rev.* 67:593–656.

32. Pier, G. B. 2000. Peptides, *Pseudomonas aeruginosa*, polysaccharides and lipopolysaccharides—players in the predicament of cystic fibrosis patients. *Trends Microbiol.* 8:247–251.

33. Knirel, Y. A., O. V. Bystrova, …, G. B. Pier. 2006. Conserved and variable structural features in the lipopolysaccharide of *Pseudomonas aeruginosa*. *J. Endotoxin Res.* 12:324–336.

34. Zhou, Z., A. A. Ribeiro, …, C. R. H. Raetz. 2001. Lipid A modifications in polymyxin-resistant *Salmonella typhimurium*: PMRA-dependent 4-amino-4-deoxy-L-arabinose, and phosphoethanolamine incorporation. *J. Biol. Chem.* 276:43111–43121.

35. Hankins, J. V., J. A. Madsen, …, M. S. Trent. 2012. Amino acid addition to *Vibrio cholerae* LPS establishes a link between surface remodeling in Gram-positive and Gram-negative bacteria. *Proc. Natl. Acad. Sci. USA.* 109:8722–8727.

36. Raoult, D., G. Aboudharam, …, M. Drancourt. 2000. Molecular identification by "suicide PCR" of *Yersinia pestis* as the agent of medieval black death. *Proc. Natl. Acad. Sci. USA.* 97:12800–12803.

37. Rebeil, R., R. K. Ernst, …, B. J. Hinnebusch. 2006. Characterization of late acyltransferase genes of *Yersinia pestis* and their role in temperature-dependent lipid A variation. *J. Bacteriol.* 188:1381–1388.

38. Montminy, S. W., N. Khan, …, E. Lien. 2006. Virulence factors of *Yersinia pestis* are overcome by a strong lipopolysaccharide response. *Nat. Immunol.* 7:1066–1073.

39. Jo, S., T. Kim, …, W. Im. 2008. CHARMM-GUI: a web-based graphical user interface for CHARMM. *J. Comput. Chem.* 29:1859–1865.

40. Jo, S., J. B. Lim, …, W. Im. 2009. CHARMM-GUI Membrane Builder for mixed bilayers and its application to yeast membranes. *Biophys. J.* 97:50–58.

41. Wu, E. L., X. Cheng, …, W. Im. 2014. CHARMM-GUI Membrane Builder toward realistic biological membrane simulations. *J. Comput. Chem.* 35:1997–2004.

42. Jo, S., E. L. Wu, …, W. Im. 2015. Lipopolysaccharide membrane building and simulation. *Methods Mol. Biol.* 1273:391–406.

43. Klauda, J. B., R. M. Venable, …, R. W. Pastor. 2010. Update of the CHARMM all-atom additive force field for lipids: validation on six lipid types. *J. Phys. Chem. B.* 114:7830–7843.

44. Guvench, O., S. N. Greene, …, A. D. MacKerell, Jr. 2008. Additive empirical force field for hexopyranose monosaccharides. *J. Comput. Chem.* 29:2543–2564.

45. Guvench, O., E. R. Hatcher, …, A. D. MacKerell. 2009. CHARMM additive all-atom force field for glycosidic linkages between hexopyranoses. *J. Chem. Theory Comput.* 5:2353–2370.

46. Guvench, O., S. S. Mallajosyula, …, A. D. MacKerell, Jr. 2011. CHARMM additive all-atom force field for carbohydrate derivatives and its utility in polysaccharide and carbohydrate-protein modeling. *J. Chem. Theory Comput.* 7:3162–3180.

47. Best, R. B., X. Zhu, …, A. D. MacKerell, Jr. 2012. Optimization of the additive CHARMM all-atom protein force field targeting improved sampling of the backbone φ, ψ and side-chain χ^1 and χ^2 dihedral angles. *J. Chem. Theory Comput.* 8:3257–3273.

48. Luo, Y., and B. Roux. 2010. Simulation of osmotic pressure in concentrated aqueous salt solutions. *J. Phys. Chem. Lett.* 1:183–189.

49. Venable, R. M., Y. Luo, …, R. W. Pastor. 2013. Simulations of anionic lipid membranes: development of interaction-specific ion parameters and validation using NMR data. *J. Phys. Chem. B.* 117:10183–10192.

50. Lee, J., X. Cheng, …, W. Im. 2016. CHARMM-GUI input generator for NAMD, GROMACS, AMBER, OpenMM, and CHARMM/OpenMM simulations using the CHARMM36 additive force field. *J. Chem. Theory Comput.* 12:405–413.

51. Brooks, B. R., C. L. Brooks, 3rd, …, M. Karplus. 2009. CHARMM: the biomolecular simulation program. *J. Comput. Chem.* 30:1545–1614.

52. Ryckaert, J. P., G. Ciccotti, and H. J. C. Berendsen. 1977. Numerical integration of Cartesian equations of motion of a system with constraints—molecular dynamics of n-alkanes. *J. Comput. Phys.* 23:327–341.

53. Phillips, J. C., R. Braun, …, K. Schulten. 2005. Scalable molecular dynamics with NAMD. *J. Comput. Chem.* 26:1781–1802.

54. Steinbach, P. J., and B. R. Brooks. 1994. New spherical-cutoff methods for long-range forces in macromolecular simulation. *J. Comput. Chem.* 15:667–683.

55. Essmann, U., L. Perera, …, L. G. Pedersen. 1995. A smooth particle mesh Ewald method. *J. Chem. Phys.* 103:8577–8593.

56. Martyna, G. J., D. J. Tobias, and M. L. Klein. 1994. Constant-pressure molecular-dynamics algorithms. *J. Chem. Phys.* 101:4177–4189.

57. Feller, S. E., Y. H. Zhang, …, B. R. Brooks. 1995. Constant-pressure molecular-dynamics simulation—the Langevin piston method. *J. Chem. Phys.* 103:4613–4621.

58. Wu, E. L., O. Engström, …, W. Im. 2013. Molecular dynamics and NMR spectroscopy studies of *E. coli* lipopolysaccharide structure and dynamics. *Biophys. J.* 105:1444–1455.

59. Wu, E. L., P. J. Fleming, …, W. Im. 2014. *E. coli* outer membrane and interactions with OmpLA. *Biophys. J.* 106:2493–2502.

60. Patel, D. S., S. Re, …, W. Im. 2016. Dynamics and interactions of OmpF and LPS: influence on pore accessibility and ion permeability. *Biophys. J.* 110:930–938.

61. Kučerka, N., M. P. Nieh, and J. Katsaras. 2011. Fluid phase lipid areas and bilayer thicknesses of commonly used phosphatidylcholines as a function of temperature. *Biochim. Biophys. Acta.* 1808:2761–2771.

62. Rawicz, W., K. C. Olbrich, …, E. Evans. 2000. Effect of chain length and unsaturation on elasticity of lipid bilayers. *Biophys. J.* 79:328–339.

63. Jo, S., T. Kim, and W. Im. 2007. Automated builder and database of protein/membrane complexes for molecular dynamics simulations. *PLoS One.* 2:e880.

64. Snyder, S., D. Kim, and T. J. McIntosh. 1999. Lipopolysaccharide bilayer structure: effect of chemotype, core mutations, divalent cations, and temperature. *Biochemistry.* 38:10758–10767.

65. van Alphen, L., A. Verkleij, …, B. Lugtenberg. 1978. Architecture of the outer membrane of *Escherichia coli*. III. Protein-lipopolysaccharide complexes in intramembraneous particles. *J. Bacteriol.* 134:1089–1098.

66. Schindler, M., and M. J. Osborn. 1979. Interaction of divalent cations and polymyxin B with lipopolysaccharide. *Biochemistry.* 18:4425–4430.

67. Coughlin, R. T., S. Tonsager, and E. J. McGroarty. 1983. Quantitation of metal cations bound to membranes and extracted lipopolysaccharide of *Escherichia coli*. *Biochemistry.* 22:2002–2007.

68. Lindblom, G., and G. Orädd. 2009. Lipid lateral diffusion and membrane heterogeneity. *Biochim. Biophys. Acta.* 1788:234–244.

69. Rassam, P., N. A. Copeland, …, C. Kleanthous. 2015. Supramolecular assemblies underpin turnover of outer membrane proteins in bacteria. *Nature.* 523:333–336.

70. Impey, R. W., P. A. Madden, and I. R. McDonald. 1983. Hydration and mobility of ions in solution. *J. Phys. Chem.* 87:5071–5083.

71. van der Bruggen, B., A. Koninckx, and C. Vandecasteele. 2004. Separation of monovalent and divalent ions from aqueous solution by electrodialysis and nanofiltration. *Water Res.* 38:1347–1353.

72. Cañadas, O., K. M. W. Keough, and C. Casals. 2011. Bacterial lipopolysaccharide promotes destabilization of lung surfactant-like films. *Biophys. J.* 100:108–116.

73. Cantor, R. S. 1997. The lateral pressure profile in membranes: a physical mechanism of general anesthesia. *Biochemistry.* 36:2339–2344.

74. Cantor, R. S. 1999. Lipid composition and the lateral pressure profile in bilayers. *Biophys. J.* 76:2625–2639.

75. Sodt, A. J., and R. W. Pastor. 2014. Molecular modeling of lipid membrane curvature induction by a peptide: more than simply shape. *Biophys. J.* 106:1958–1969.

76. Harasima, A. 1958. Molecular theory of surface tension. *Adv. Chem. Phys.* 1:203–237.

77. Sonne, J., F. Y. Hansen, and G. H. Peters. 2005. Methodological problems in pressure profile calculations for lipid bilayers. *J. Chem. Phys.* 122:124903.

78. Park, S., A. H. Beaven, …, W. Im. 2015. How tolerant are membrane simulations with mismatch in area per lipid between leaflets? *J. Chem. Theory Comput.* 11:3466–3477.

79. Mingeot-Leclercq, M. P., and J. L. Decout. 2016. Bacterial lipid membranes as promising targets to fight antimicrobial resistance, molecular foundations and illustration through the renewal of aminoglycoside antibiotics and emergence of amphiphilic aminoglycosides. *MedChemComm.* 7:586–611.